Strain-dependent characterization of electrode and polymer network of electrically activated polymer actuators

Tino Töpper[a], Bekim Osmani[a], Florian M. Weiss[a,b], Carla Winterhalter[a], Fabian Wohlfender[a], Vanessa Leung[a], and Bert Müller*[a]
[a]Biomaterials Science Center, University of Basel, c/o University Hospital, 4031 Basel, Switzerland;
[b]Swiss Federal Laboratories for Materials Science and Technology, Überlandstrasse 129, 8600 Dübendorf, Switzerland

ABSTRACT

Fecal incontinence describes the involuntary loss of bowel content and affects about 45 % of retirement home residents and overall more than 12 % of the adult population. Artificial sphincter implants for treating incontinence are currently based on mechanical systems with failure rates resulting in revision after three to five years. To overcome this drawback, artificial muscle sphincters based on bio-mimetic electro-active polymer (EAP) actuators are under development. Such implants require polymer films that are nanometer-thin, allowing actuation below 24 V, and electrodes that are stretchable, remaining conductive at strains of about 10 %. Strain-dependent resistivity measurements reveal an enhanced conductivity of 10 nm compared to 30 nm sputtered Au on silicone for strains higher than 5 %. Thus, strain-dependent morphology characterization with optical microscopy and atomic force microscopy could demonstrate these phenomena. Cantilever bending measurements are utilized to determine elastic/viscoelastic properties of the EAP films as well as their long-term actuation behavior. Controlling these properties enables the adjustment of growth parameters of nanometer-thin EAP actuators.

Keywords: Compliant electrode, ultra-thin gold-film resistivity, four-point conductivity measurement, cantilever bending, asymmetric planar electro active polymer, polyetheretherketone, polydimethylsiloxane, viscoelasticity

1. INTRODUCTION

The changing demographics of modern society have resulted in the increasing prevalence of socially and economically significant, age-related diseases. Among them is a loss of control of the defecation process, also known as fecal incontinence (FI) [1]. FI encompasses all forms of involuntary loss of bowel content, including flatus, mucus, liquid and solid feces. In adults, the overall prevalence of FI is between 11 and 15 % [1] and increases with age [2]. Approximately one third of individuals in retirement homes or similar institutions are affected [2]. FI prevalence in retirement homes in the U.S. is about 45 % [3, 4], a figure which agrees with those found in European cross-sectional studies [5]. Individuals with FI experience detrimental effects, which include the exclusion from social life, isolation and stigmatization [1], and economic impact [2].

Artificial sphincter implants offers a possible solution to treat severe fecal incontinence. Yet, it remains a significant challenge for the researchers to build artificial muscles to reproduce the capabilities of the natural sphincter [6]. Currently available implants show long-term re-operation rates of 95 % and definitive ex-plantation rates of 40 %. The high risk of failure excludes these implants from everyday surgery. Electrically activated polymer (EAP) actuators can potentially fill the pressing need for a bio-mimetic implant [6]. Technical advantages of EAPs include their versatility, response time, forces, and energy consumption [7]. Biomimetic artificial sphincters based on EAPs will support a rapidly adaptive pressure response, comparable to the natural feedback mechanism of the human body.

An artificial sphincter device might be actuated by an EAP-based sandwiched nanostructure and controlled by an implantable battery-powered microcomputer re-charged using the power of the human body. The innovation lies in the avoidance of constant compression and therefore erosion of the tissue. For example, a series of shutter modules work over a pre-defined length of the digestive tube or the urethra and should open and close in a certain time sequence.

*bert.mueller@unibas.ch; phone 41 61 265 9660; fax 41 61 265 9699; www.bmc.unibas.ch

Electroactive Polymer Actuators and Devices (EAPAD) 2015, edited by Yoseph Bar-Cohen, Proc. of SPIE
Vol. 9430, 94300B · © 2015 SPIE · CCC code: 0277-786X/15/$18 · doi: 10.1117/12.2084595

To employ EAP structures as active and powered implants, voltages should not exceed the medically acceptable range of 24 V. Multi-layer stacks allow the actuation of multiple low-voltage dielectric EAP structures with a thickness in the nanometer regime to be harnessed in parallel. Such stacking results in an effective actuation comparable to that of currently available high-voltage EAP structures with a thickness in the micrometer range. Yet, the impact of the Young's modulus of the metal on the effective modulus of the entire EAP structure is pronounced in multi-stack actuators, even if the electrodes are much thinner than the polymer layer. Compliant electrodes that do not dominate the stiffness of the entire structure have yet to be clearly identified, although several potential candidates exist. Bi-layer systems of soft polymer bulk material and rigid thin-layered coatings have been studied for applications in packaging and microelectronics. It has thus been found, for example, that ultra-thin noble metal films on polymers including polydimethylsiloxane (PDMS) give rise to strains well above 10 % [8].

For the optimization of polymer films as well as the ultra-thin metal layer electrodes in dielectric electro active actuators (DEA)-microstructures, several measurement techniques must be employed. In our case, a combination of two techniques allows the electrical and mechanical properties of the actuators to be quantified. The electrical conductivity of the electrodes is essential for the response time of the actuator and must be characterized for the optimized performance of the engineered artificial muscle. Four-point measurement is a well-established technique that allows the measurement of the electrode resistivity [9-12].

In addition, mechanical properties such as elasticity and viscoelasticity are crucial for the success of an EAP actuator. Cantilever-bending measurements are based on an established technique used in a broad range of applications, for example atomic force microscopy [13-18]. We have previously demonstrated that cantilever bending is a method well suited to evaluate EAP microstructures with high angular resolution at low voltages [19, 20]. Finally, qualitative knowledge of the morphological details can support the quantitative results obtained by the four-point conductivity and cantilever-bending measurements. The morphology of the substrate is characterized through the combination of optical microscopy and atomic force microscopy.

2. EXPERIMENTAL

2.1 Cantilever preparation

The asymmetric EAP-microstructures evaluated were built on polyetheretherketone (PEEK) substrates (APTIV 2000, Victrex, Lancashire, UK) with a thickness of 25 µm or the n-doped Si-wafers with a thickness of (20 ± 10) µm from Wafer World Inc., West Palm Beach FL, USA. The PEEK films were cut to the dimensions of a 3-inch wafer. The substrates were cleaned with acetone (Merck KGaA, Darmstadt, Germany). Subsequently, gold (Lesker, East Sussex, UK) was magnetron-sputtered on the rougher side of the PEEK film, mean surface roughness about 0.8 µm, or on the polished side of the Si wafer under vacuum conditions at room temperature. The related sputtering conditions in the Balzers Union SCD 040 system (Balzers, Lichtenstein) corresponded to 0.05 mbar Ar-atmosphere (Carbagas AG, Gümligen, Switzerland) and a constant working current of 30 mA. The thickness of the Au electrodes ranged from 7 to 30 nm, determined by a calibration curve plotting time versus thickness measured using a quartz crystal microbalance (QSG 301, Balzers, Balzers, Lichtenstein). In the next step, the Au-covered substrates were spin-coated using PDMS (Elastosil 745 A/B, Wacker Chemie AG, Munich, Germany) mixed in a volume ratio 1:1 (component A and B) or Sylgard 184 (DowCorning, Wiesbaden, Germany) with a ratio of 10:1 of elastomer to curing agent with rotation speeds to obtain layer thicknesses ranging from 2 to 5 µm. Before crosslinking the PDMS films at a temperature of 120 °C for a duration of 30 to 120 minutes, the coated substrates were partly submerged into ethyl acetate (Fisher Scientific, Reinach, Switzerland) to dissolve and wash off the PDMS in order to become access to the lower electrode as described previously [21]. After PDMS-crosslinking, a mask covered some parts of the structure to obtain two electrodes with a step-like profile as displayed in Figure 5 of Ref. [22]. The uncovered PDMS surfaces were then sputter-coated with Au under the comparable conditions as the first electrode.

2.2 Bending measurement

In principle, the operation mode of electrically activated polymer (EAP) structures is based on the COULOMB attraction between positively and negatively charged electrodes embedding a dielectric elastomer such as silicone or acrylic based polymers. If a voltage is applied the two electrodes become oppositely charged and due to the attraction force squeeze the elastomer layer in *z*-direction, whereas the area increases because the volume is assumed to remain constant. Thus, an voltage-dependent expansion in *x*- and *y*-directions can be observed.

In case of an asymmetric planar structure such as a cantilever-shaped structure the applied strain will induce a torque, which results in a bending of the structure if one end is fixed on a mount while the other one freely moves [20]. To isolate the EAP-microstructure electrically, a Teflon mount was chosen. The voltage was applied via wires coated with drops of fluid metal (Coollaboratory Liquid Pro, Coollaboratory, Magdeburg, Germany). The bending can be recorded by a position sensitive detector (PSD), which detects the displacement of the reflected laser beam as described previously [20, 21]. To avoid disturbance of this sensitive displacement detection by external acoustic, motional, and thermal influences the entire setup is sealed within an aluminum box [22].

2.3 Four-point conductance measurement on soft substrates

To quantify the sheet resistance R_s of the conducting electrode layer we used the well-established four-point method, schematically shown in part (a) of Figure 1 [10, 11]. In contrast to two-terminal sensing the advantage of four-terminal sensing is that the resistances of wires, contacts and the internal resistance of ampere meter and voltage source will not influence the result, since the current does not circulate through the electrodes returning the voltage difference [11]. Applying current I through two point-like outer contacts on an infinite plane gives rise to an electrostatic potential $\phi(r)$. If this potential is measured at the two inner contacts and the four contacts are aligned equally spaced on a straight line, the resulting voltage difference can be written according to Ref. [23]:

$$U = \phi(r_1) - \phi(r_2) = \frac{\ln(2)}{\pi} R_s I \tag{1}$$

Since the sample is finite and the current- and voltage-connecting tips are not infinitesimally small, geometric effects must be considered [10]. Therefore, the Hall-bar symmetry (see scheme part (a) of Figure 1) was applied to determine the dependence between resistance and electrode thickness of Au on PDMS. The voltage drop is measured at two contacts not lying in the current flow. Therefore, effects due to tip sizes are negligible. The resistance of a Hall bar of length L and width W is obtained by

$$R_s = \frac{U}{I}\frac{W}{L} \tag{2}$$

To determine the strain-dependent resistance, a circularly shaped Au layer with a diameter of 37 mm was deposited on PDMS, which was spin-coated on a VHB F9460PC film (3M, St. Paul, USA) and subsequently mounted on a translation stages to be stretched. The distance s between the tips was set to 5 mm. Correction factors are available to compensate for the round shape of the layer [12]. If the four-point probe is centered and the tips are equally spaced with distance s, the voltage drop on a circularly shaped sample with diameter d is:

$$U = \frac{IR_s}{\pi}\left[\ln(2) + \ln\left(\frac{(\frac{d}{s})^2 + 3}{(\frac{d}{s})^2 - 3}\right)\right] \tag{3}$$

The setup did consist of four semi-spherical probe tips (SPA-3J, Everett Charles Technologies, Distrilect) mounted on micro positioners (Signatone, aps Solutions GmbH, Munich, Germany) to place the measurement tips on the specimen individually. A non-destructible contact between tip and specimen was realized by adding a liquid metal drop onto the tip (Coollaboratory Liquid Pro, Coollaboratory, Magdeburg, Germany). To apply current and determine the voltage drop, a commercially available source meter (Keithley 2401) and a multimeter (Agilent 34461A Truevolt) were employed. For the measurements a constant current of 10 mA was chosen. The variation of voltage was detected.

2.4 Imaging of EAP-electrodes

The Au surface was imaged with an optical light microscope (Stemi DV4 SPOT, Carl Zeiss AG, Feldbach, Switzerland) using an optical magnification of 50. For higher spatial resolution an atomic force microscope (AFM), FlexAFM ARTIDIS system, Nanosurf AG, Liestal, Switzerland, was applied. Here, areas of 97.5 µm × 97.5 µm (512 × 512 points) were recorded in tapping mode with a Tap150AI-G tip (Budget Sensors, Innovative Solutions Bulgaria Ltd., Sofia, Bulgaria). For visualization purposes mean plane subtraction was applied using the Gwyddian software (Department of Nanometrology, Czech Metrology Institute, Brno, Czech Republic).

3. RESULTS

3.1 Thickness- and strain-dependent resistivity of nanometer-thin Au electrodes on PDMS

Figure 1 represents experimental data of the four-point measurements for Au on PDMS. Part (b) includes the dependence of the bulk resistivity to the layer thickness determined within the Hall-bar symmetry, as sketched in part (a). The relation between measured resistance R_s, according to Equation 2, and the bulk resistivity ρ is simply the product of resistance and electrode thickness d [10].

$$\rho = R_s d \tag{4}$$

For Au thicknesses larger than 14.0 nm a constant bulk resistivity of $(1.4 \pm 0.2)\ 10^{-7}$ Ωm was observed. Although the resistance increases from (6.7 ± 0.7) via (7.5 ± 0.8) to (10.4 ± 1.1) Ω for 21.0, 17.5 and 14.0 nm, respectively, their product stays constant. A further reduction of the Au layer thickness, however, leads to a larger increase of their resistance, i.e. (22 ± 2) and (103 ± 11) Ω for 10.5 and 7.0 nm. Additionally, a remarkable increase of the bulk resistivity to (2.31 ± 0.22) and $(7.21 \pm 7.80)\ 10^{-7}$ Ωm is obtained.

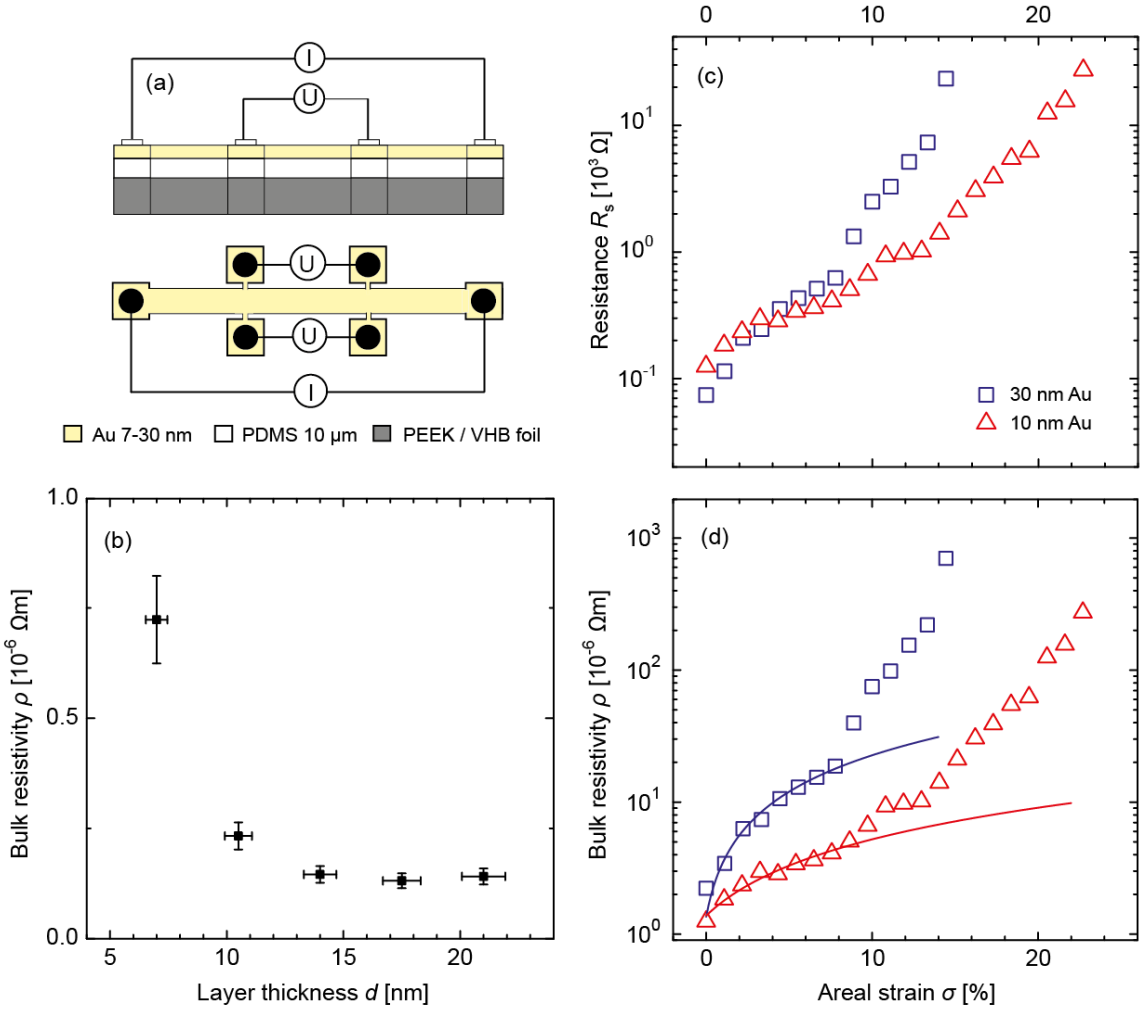

Figure 1. (a - b) The four-point resistance measurements of sputtered Au layers on PDMS are shown. The Hall-bar symmetry was chosen to exclude the influence of the contact resistance through the tips. The bulk resistivity ρ is comparable to the literature values of 0.2×10^{-6} Ωm for stress-free gold layers on PET [24] if no stress is applied. (c - d) The strain dependence of resistance R_s and bulk resistivity ρ was determined with a four-point measurement on a 60 mm × 60 mm VHB film for 30 and 10 nm-thin Au films on PDMS. A maximal areal strain of up to 23 % in one lateral direction of the multilayer stack was applied. The fits illustrate the linear behavior of the bulk resistivity for areal strains up to 8 %.

Parts (c) and (d) of Figure 1 present strain-dependent resistance and resistivity data of 10 and 30 nm-thin Au films on PDMS. An in-line setup of four tips each 5 mm apart was fixed, whereas the sample mounted on a VHB-film was stretched. For this setup, the resistance was calculated according to Equation 3. In a relaxed state a 1.5 times lower resistance for 30 compared to 10 nm-thin Au layer was detected. Both, the 10 and 30 nm-thin Au layers exhibit a bulk resistivity, which is at least one order of magnitude higher than for thicker Au layers on PDMS deposited on PEEK. This behavior might be due to the flexibility and related morphology changes before the controlled areal strain could be applied.

When a lateral strain is applied to this multilayer stack a rise of resistance is monitored. Here, the slope for the 30 nm-thin layers is larger than for the 10 nm-thin layers on PDMS. At an areal strain above 5 % the 30 nm-thin Au layer exhibits a higher resistance than the 10 nm-thin Au layer on strained PDMS. The translation of resistance into bulk resistivity according to Equation 4 reveals a linear slope for the resistivity with increasing strain of up to 8 %. For the thicker Au film this slope was found to be 5.6 times higher than for the thinner one, cp. (2.13 ± 0.09) vs. $(0.38 \pm 0.03)\ 10^{-6}\ \Omega m$. At 13 % areal strain the 30 nm-thin Au layer shows a two orders of magnitude higher resistivity with respect to the 10 nm-thin Au layer.

One might expect that the changes in the conductance relate to the surface morphology. Therefore, 20 % areal strain was applied to the 10 and 30 nm-thin Au films on PDMS and optical micrographs, as shown in Figure 2, captured. The strain was applied in horizontal direction of the image orientation. The images with selected magnifications illustrate the relaxation behavior of the EAP-structures under strain.

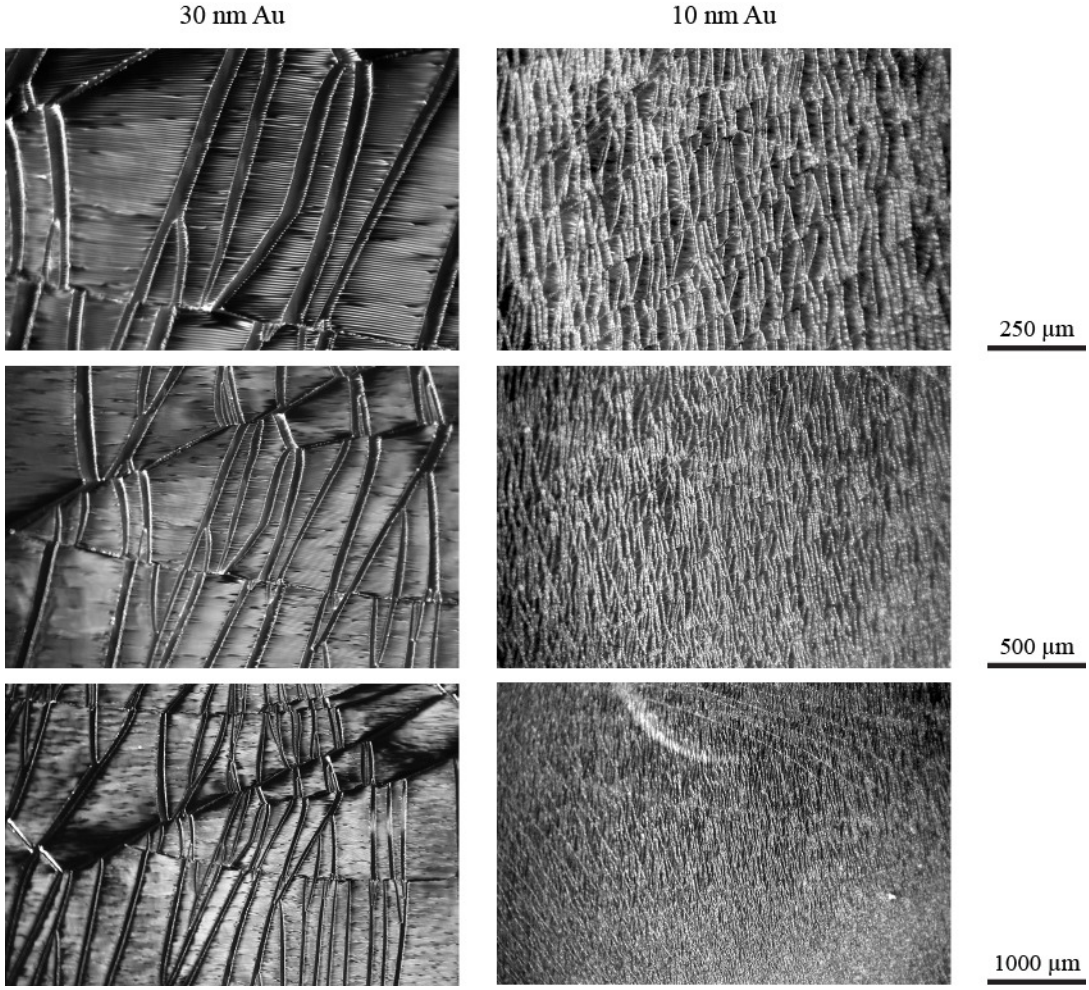

Figure 2. Optical micrographs of 30 nm (left side) and 10 nm (right side) thin Au-layers sputtered on PDMS on top of stretched VHB-films are shown. Horizontally to the images shown, 20 % areal strain was applied.

The 30 nm-thin Au layer forms islands of millimeter size. Cracks of up to 30 µm in horizontal direction occur. At the same strain level, the 10 nm-thin Au shows smaller islands and cracks with a width of only a very few micrometers. The images with lowest magnification in Figure 2 reveal the average crack densities, i.e. 4 and 30 mm^{-1} for the thicker and thinner Au-layers, respectively.

The AFM images represented in Figure 3 give a more detailed insight into the surface morphology of the Au-layers. In the relaxed state, the surfaces appear smooth. The features up to 60 nm high are attributed to dust particles common if the layers are prepared under ambient conditions. After the application of 20 % areal strain one also recognizes the five to ten micrometers wide cracks on the 10 nm-thin Au layer. The AFM data, however, also show horizontally orientated wrinkles with the height of 1.1 and 2.2 µm for 10 and 30 nm-thin Au-layers, respectively. This microstructure is probably a result of the shrinking of the VHB film in vertical direction to compensate for the stretching in horizontal direction. For thicker Au-layers the amplitude of the wrinkles is not only two times larger but also their width of approximately 9.0 µm is significantly larger with respect to the value found for the 10 nm-thin Au-layers, i.e. 2.3 µm.

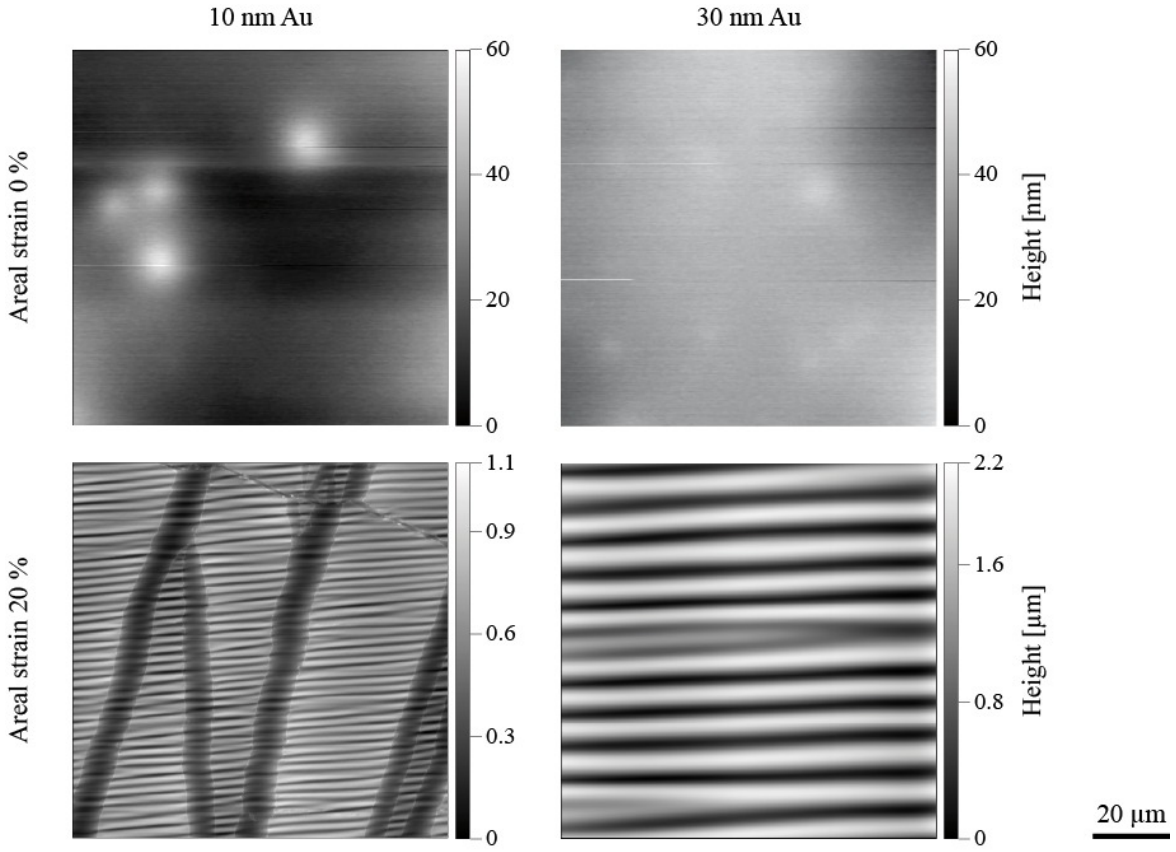

Figure 3. The AFM images of 30 and 10 nm-thin Au-layers sputtered on PDMS demonstrate the effect of applying 20 % areal strain in horizontal direction to the image. One finds periodically arranged wrinkles of micrometer size.

3.2 Elastic properties of EAPs determined by cantilever bending

For the actuation analysis of EAP microstructures the cantilever bending method is a powerful tool to access the elastic properties. For example, one can study the actuation as the function of polymerization time. The curvature of the cantilever depends on the applied voltage, as for example shown in Figure 4. EAP actuators based on Elastosil A/B, embedded between 15 nm-thin Au electrodes, and deposited on 25 µm-thick PEEK films were heat cured for 1.8×10^3 s (0.5 h) and 7.2×10^3 s (2 h), respectively. Subsequently, an actuation voltage of 200 and 400 V was applied for a period of 80 s. The actuator cured for the shorter period of time (0.5 h) showed more than doubled deflection compared to the other actuator. Nevertheless, its actuation dropped within a period of 10 to 20 s to a lower but stable value. This relaxation process can be characterized by the time constant τ, which was determined by an exponential fit function to $\tau = (2.93 \pm 0.03)$ s, see Figure 4. For actuator heat-cured for two hours no such relaxation behavior was observed.

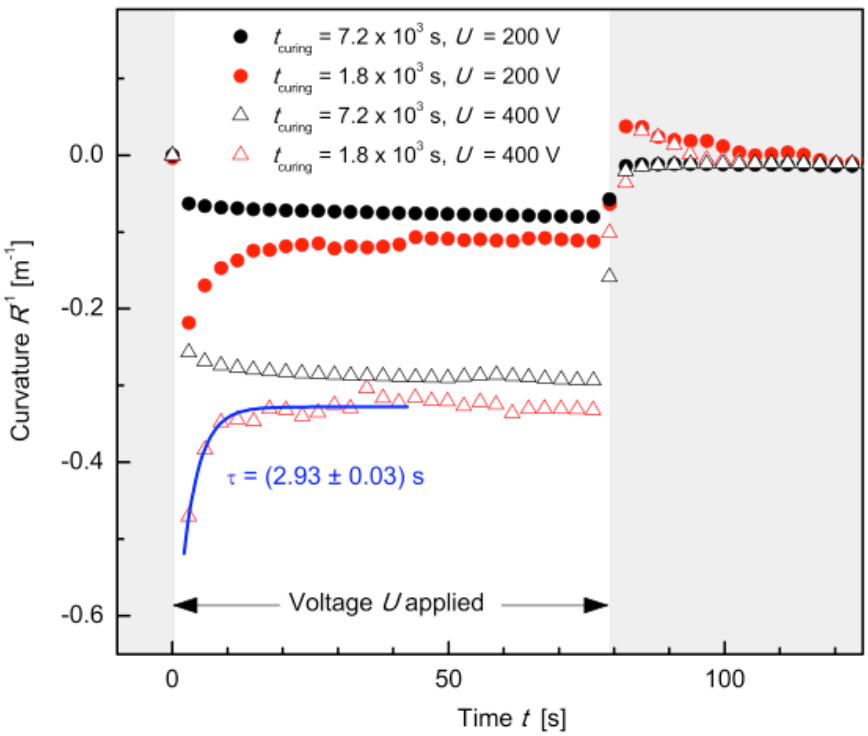

Figure 4. The actuation behavior of EAP-microstructures on PEEK cantilevers is presented for actuation voltages of 200 and 400 V and compared for curing times of 1.8 and 7.2 10^3 s (0.5 and 2.0 h), respectively. Heat curing of the Elastosil A/B layers at a temperature of 120 °C seems to be incomplete, if the curing time is restricted to half an hour. Nevertheless, the actuation is larger for the incompletely cured layers than for the fully polymerized elastomer.

It is worth mentioning that a certain period of time, which is about 10 s, is required to observe the maximal curvature. A similar phenomenon is found, when the voltage is switched off, cp. Figure 4.

To gain a more detailed insight to the actuation as the function of the curing time, the period for curing was set to 1.2, 1.8, 2.4, 3.6 10^3 s. The corresponding time constants for relaxation were derived and are summarized in Table 1. This table also contains the ratios between the maximal bending and the one measured after equilibration. As expected, the relative actuation relaxation values decrease and the time constants increase as the curing time is extended.

Table 1. Relaxation parameters obtained from an asymmetric EAP-structures based on Elastosil A/B, see section 2.2, heat cured at a temperature of 120 °C for a period between 1.2 and 3.6 10^3 s, i.e. 20 to 60 minutes. The presented relaxation characteristics were determined at an actuation voltage of 400 V, which corresponds to a Maxwell strain of 22 %.

Time of heat curing [10^3 s]	τ [s]	Actuation relaxation [%]
1.2	0.32 ± 0.01	93 ± 1
1.8	2.9 ± 0.6	43 ± 2
2.4	14 ± 2.8	36 ± 4
3.6	60 ± 24	14 ± 2

3.3 Actuation characteristics determined by multi-cycle cantilever bending

The cantilever bending induced by EAP-actuators on top of a polymeric substrate including PEEK has been successfully applied to characterize the electrode properties [21]. Nevertheless, reasonable reliability tests over a longer period of time and a related number of cycles require stability of the experimental setup and the EAP-structure. Therefore, the actuation characteristics of EAP-structures consisting of 2 µm-thin PDMS (Sylgard®184 silicone elastomer, Dow Corning Corporation, Midland MI, USA) with 20 nm-thin sputtered Au electrodes on single-crystal 20 µm-thick Si substrates were measured. The curvature of the cantilever directly yields the actuation amplitude. Figure 5 displays the results as a function on the cycle number and the time (logarithmic scale). For an applied voltage of 32 V the actuation is initially increasing until the electrodes of the EAP-structures are fully charged. During the actuation polymer and electrodes develop a characteristic defect structure associated with changes in the actuation amplitude. After about 300 actuation cycles the changes become negligible. Applying a three times higher actuation voltage, i.e. 96 V, one also observes this behavior with a steady state level reached at 1,600 cycles.

Printing the time scale in logarithmic fashion, as given in the right diagram of Figure 5 reveals that during the first 10 s charging periods the used 96 V pulses are too short to fully load the capacity of the EAP-structure.

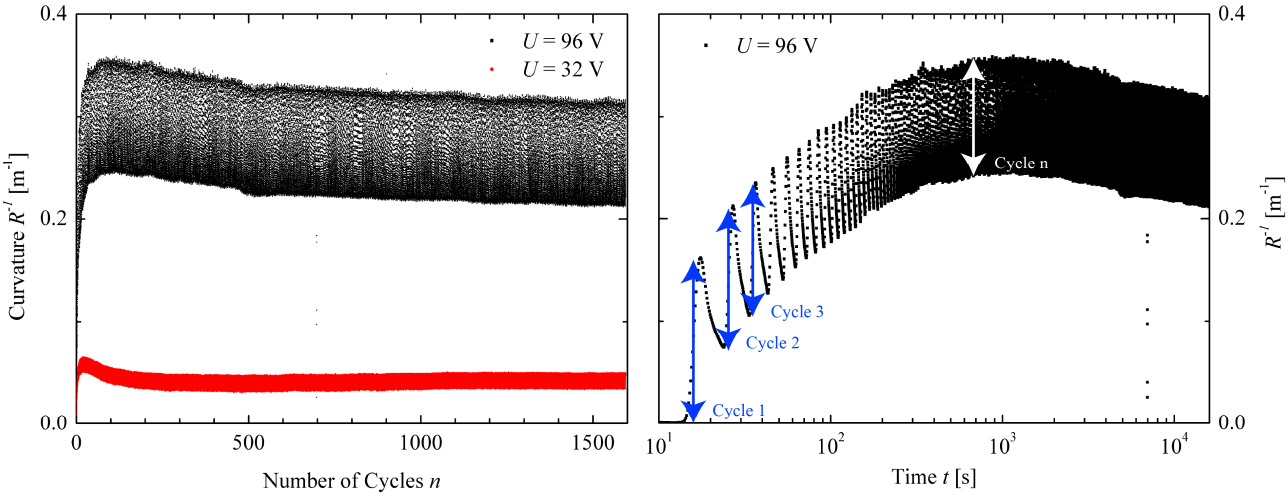

Figure 5. Bending of a 20 µm-thin Si cantilever induced by a 2 µm-thin EAP-structure on top. Applying 1,600 pulses of 32 and 96 V with a frequency of 0.1 Hz, the curvature changes in a characteristic manner. The charging and discharging of the EAP-structure follows the conventional behavior of the resistance-capacitance circuit. Thus, the EAP-actuator is fully charged after a number of cycles, given by the pulse frequency.

4. DISCUSSION

The four-point conductivity measurements on nanometer-thin Au films revealed the expected increase of sheet resistance with decreasing layer thickness. Nevertheless, the related bulk resistivity was found to stay constant for a film thickness down to 14 nm, implying that Au films on polymeric substrates with thicknesses above that level keep their bulk-like conductivity behavior. For a smaller thickness, a remarkable increase of the bulk resistivity was detected, concluding that a continuity of the Au film cannot be assumed [24]. The findings correspond to the measured bulk resistivity of 50 nm-thin Au on PDMS with 3.5 10^{-7} Ωm [9] and 2 10^{-7} Ωm for 21 nm-thin Au on polyethylene terephthalate (PET) [24]. The transition thickness, at which the step-like increase of bulk resistivity occurs, was found between 5 and 7 nm for Au on PET [25]. The difference to the data in the present communication, i.e. between 10.5 and 14.0 nm for Au on PDMS, is probably a result of the surface morphology and defect structure of the Au film, which depend on the substrate film and the deposition parameters. It should be noted that the layer resistivity above the transition thickness is about one order of magnitude higher than that of bulk gold, i.e. 2 10^{-8} Ωm [26]. The low thickness values, related to less compact arrangements of the Au atoms, justify the difference derived.

In the range up to 8 % areal strain the strain-dependent resistivity measurements revealed a significantly greater linear increase for 30 nm-thin Au film than for the 10 nm-thin one. Optical micrographs have evidentially shown that for the thicker Au film larger cracks occur and thus hinder the current flow in the direction of applied strain. At 20 % areal

strain the thinner Au film exhibited a crack density of 30 mm^{-1}, more than a factor of seven larger than for the three times thicker Au film. It becomes therefore clear that the more compact and bulk-like Au film is the less adaptable to the substrate under strain. The larger crack width between the islands of the thicker Au film results in the steeper slope of the resistivity as the function of the applied strain. This behavior is disadvantageous for the response time of the actuator, which is directly proportional to the resistance of the electrodes. Furthermore, it implies that during actuation micrometer-size regions form, in which no electrical charge can be deposited, thus resulting in reduced actuation efficiency. The results of Graz et al. [9] revealed that for a 50 nm-thin Au films grown on 5 nm-thin Cr the increase was found to be linear up to 20 % strain with a slope of 0.65 10^{-6} Ωm/%. This value is three times smaller than the one for the 30 nm-thin Au layer grown on PDMS.

The cantilever bending measurements allow for the characterization of the actuation response of the electrically activated polymer layer. Exemplarily, we investigated dielectric actuators based on heat-cured Elastosil A/B. The polymer film shows a curing-time dependent compliance under strain. Increasing the curing time of the polymer layer the relaxation process of the actuation decreases. Simultaneously, the relaxation is slowed down, which we quantified by means of a time constant. As the completely cross-linked PDMS layers are known to be incompressible, we can attribute the observed change of actuation response to the degree of cross-linking within the polymer network. Consequently, the cantilever bending method enables us to assess the viscoelastic response of polymer thin films to the applied MAXWELL strain. It represents a promising alternative to the established characterization of thermal wrinkling of confined polymer films [27] in order to determine the elastic and viscoelastic properties of micrometer-thin films.

Furthermore, we performed multiple-actuation cycling of the dielectric structures on single-crystalline Si cantilever substrates. The bending of the cantilever was reliably recorded for several hundred charging cycles with a frequency of 0.1 Hz. One observes, however, temporal changes in amplitude and characteristic offsets, which depend on the applied voltage. Although we cannot explain the related phenomena in quantitative fashion, we believe that a combination of reasons can be assigned. Reordering of atoms and molecules within the electrode and polymer layers occur. In addition, the n-doped Si substrate with the native oxide on top could be charged as the result of the applied voltage pulses. This phenomenon could also explain the high level of deflection, which is well above the predicted values by STONEY formula [20]. The hypothesis, that the 20 or 30 nm-thin SiO_2-layer acts as solid dielectric and generates an additional torque on the substrate, has to be proven, but sounds reasonable.

5. CONCLUSIONS

From the strain-dependent conductivity measurements we conclude that 10 nm-thin Au electrodes are a reasonable choice, although they show a resistivity twice as high as films thicker than 14 nm. Optical and AFM imaging served for the visualization of the defect structure of the thin-film Au electrodes. These images, that show a network of cracks, allow for an explanation of the electrode-thickness-dependent actuation characteristics for strains of up to 20 %.

We have demonstrated that the cantilever bending approach enables the measurement of the mechanical properties of the partially polymerized silicone films, which were heat-cured for selected periods of time. The actuation response can quantitatively be described using the decay constant and the total relaxation of actuation, both dependent on the degree of cross-linking of the confined micrometer-thin polymer film.

The cantilever bending approach also yields the voltage-dependent characteristics of multi-cycle actuation with a frequency of for example 0.1 Hz. For the single-crystalline Si substrate we identified actuation amplitudes that are higher than expected. The characteristic temporal behavior includes a relaxation of the maximum deflection with increasing number of actuation cycles, a phenomenon equally pronounced for the applied voltages. The detailed understanding of these observations need further research activities.

ACKNOWLEDGMENTS

The authors are grateful to Prof. Dr. Thomas Ihn, Physics Department, ETH Zurich, Switzerland, for the detailed discussions and advice concerning the conductivity measurements. The financial support of the Swiss National Science Foundation (project 200021-135496) and the nano-tera.ch initiative *SmartSphincter* is gratefully acknowledged. Furthermore, the authors thank VICTREX for supporting us with PEEK films.

REFERENCES

[1] Macmillan, A. K., Merrie, A. E., Marshall, R. J., and Parry, B. R., "The prevalence of fecal incontinence in community-dwelling adults: a systematic review of the literature," Diseases of the Colon and Rectum **47**(8), 1341-1349 (2004).

[2] Stoker, J., Halligan, S., and Bartram, C. I., "Pelvic floor imaging," Radiology **218**(3), 621-641 (2001).

[3] Dey, A. N., [Characteristics of elderly nursing home residents: Data from the 1995 National Nursing Home Survey] US Department of Health and Human Services, Centers for Disease Control and Prevention, National Center for Health Statistics, (1997).

[4] Nelson, R., Furner, S., and Jesudason, V., "Fecal incontinence in Wisconsin nursing homes," Diseases of the Colon and Rectum **41**(10), 1226-1229 (1998).

[5] Saga, S., Vinsnes, A., Morkved, S., Norton, C., and Seim, A., "Prevalence and correlates of fecal incontinence among nursing home residents: a population-based cross-sectional study," BMC Geriatrics **13**(1), 87 (2013).

[6] Müller, B., Deyhle, H., Mushkolaj, S., and Wieland, M., "The challenges in artificial muscle research to treat incontinence," Swiss Medical Weekly **139**, 591-595 (2009).

[7] Pelrine, R., Kornbluh, R., Pei, Q., and Joseph, J., "High-speed electrically actuated elastomers with strain greater than 100%," Science **287**(5454), 836-839 (2000).

[8] Habrard, F., Patscheider, J., and Kovacs, G., "Super-compliant metallic electrodes for electroactive polymer actuators," Proc. of SPIE **8340**, 834013 (2012).

[9] Graz, I. M., Cotton, D. P. J., and Lacour, S. P., "Extended cyclic uniaxial loading of stretchable gold thin-films on elastomeric substrates," Applied Physics Letters **94**(7), 071902 (2009).

[10] Smits, F. M., "Measurement of sheet resistivities with the four-point probe," Bell System Technical Journal **37**(3), 711-718 (1958).

[11] Valdes, L. B., "Resistivity measurements on germanium for transistors," Proc. of IRE **42**(2), 420-427 (1954).

[12] Wang, Y., Schimpf, P. H., Haynor, D. R., and Yongmin, K., "Geometric effects on resistivity measurements with four-electrode probes in isotropic and anisotropic tissues," IEEE Transactions on Biomedical Engineering **45**(7), 877-884 (1998).

[13] Binnig, G., Quate, C. F., and Gerber, C., "Atomic Force Microscope," Physical Review Letters **56**(9), 930-933 (1986).

[14] Gimzewski, J. K., Gerber, C., Meyer, E., and Schlittler, R. R., "Observation of a chemical reaction using a micromechanical sensor," Chemical Physics Letters **217**, 589-594 (1994).

[15] Köser, J., Gaiser, S., and Müller, B., "Contractile cell forces exerted on rigid substrates," European Cells and Materials **21**, 479-487 (2011).

[16] Meyer, G., and Amer, N. M., "Novel optical approach to atomic force microscopy," Applied Physics Letters **53**(12), 1045-1047 (1988).

[17] Urwyler, P., Häfeli, O., Schift, H., Gobrecht, J., Battiston, F., and Müller, B., "Disposable polymeric micro-cantilever arrays for sensing," Procedia Engineering **5**, 347-350 (2012).

[18] Urwyler, P., Schift, H., Gobrecht, J., Häfeli, O., Altana, M., Battiston, F., and Müller, B., "Surface patterned polymer micro-cantilever arrays for sensing," Sensors and Actuators A: Physical **172**(1), 2-8 (2011).

[19] Weiss, F. M., Deyhle, H., Kovacs, G., and Müller, B., "Designing micro- and nanostructures for artificial urinary sphincters," Proc. of SPIE **8340**, 83400A (2012).

[20] Weiss, F. M., Zhao, X., Thalmann, P., Deyhle, H., Urwyler, P., Kovacs, G., and Müller, B., "Measuring the bending of asymmetric planar EAP structures," Proc. of SPIE **8687**, 86871X (2013).

[21] Weiss, F. M., Töpper, T., Osmani, B., Winterhalter, C., and Müller, B., "Impact of electrode preparation on the bending of asymmetric planar electro-active polymer microstructures," Proc. of SPIE **9056**, 905607 (2014).

[22] Osmani, B., Töpper, T., Deschenaux, C., Nohava, J., Weiss, F. M., Leung, V., and Müller, B., "Micro- and nanostructured electro-active polymer actuators as smart muscles for incontinence treatment," AIP Conference Proceedings **1646**, 91-100 (2015).

[23] Ihn, T., [Semiconductor nanostructures: Quantum states and electronic transport] Oxford University Press, (2010).

[24] Svorcik, V., Zehentner, J., Rybka, V., Slepicka, P., and Hnatowicz, V., "Characterization of thin gold layers on polyethyleneterephthalate: transition from discontinuous to continuous, homogenous layer," Applied Physics A **75**(4), 541-544 (2002).

[25] Panchuk, D. A., Bazhenov, S. L., Bol'shakova, A. V., Yarysheva, L. M., Volynskii, A. L., and Bakeev, N. F., "Correlation between structure and stress-strain characteristics of metallic coatings deposited onto a polymer by the method of ionic plasma sputtering," Polymer Science Series A **53**(3), 211-216 (2011).

[26] Hodgman, C. D., [Handbook of Chemistry and Physics], Cleveland(1975).

[27] Chan, E. P., Page, K. A., Im, S. H., Patton, D. L., Huang, R., and Stafford, C. M., "Viscoelastic properties of confined polymer films measured via thermal wrinkling," Soft Matter **5**(23), 4638-4641 (2009).